Numerical Analysis of Aerodynamic Heating on Asteroid During Entry to Earth's Atmosphere

Su Siyao, Liu Sen, Dang Leiling, Zhang Zhigang

Hypervelocity Aerodynamics Institute
China Aerodynamics Research and Development Center

Outline

1、Background

2、Numerical method and physical-chemical model

3、Results and discussion

4、Summary

Outline

1、Background

2、Numerical method and physical-chemical model

3、Results and discussion

4、Summary

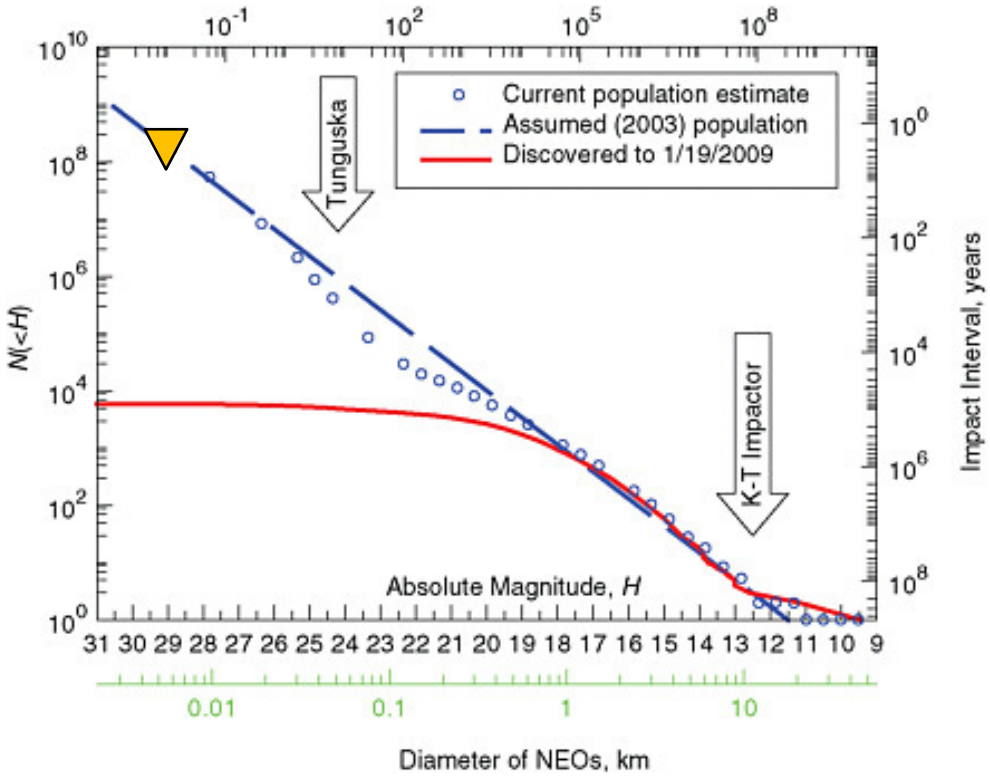

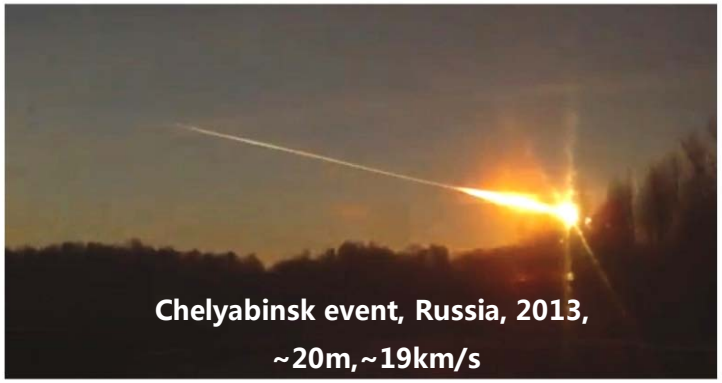
Chelyabinsk event, Russia, 2013,
~20m,~19km/s


K/T event, Chicxulub, Mexico,
65 millions years ago,
~10km,~14km/s

Meteorites in China

- **Jilin meteorites: 1976.3.8,** 3000 meteorites of total 2 ton mass have been recovered , one of the meteorites weighed as much as 1770kg.
- **Shangri-La, Yunnan: 2017.10.4 ,** many videos recorded.
- **Xishuangbanna, Yunnan: 2018.6.1 ,** many videos recorded.
- **Song Yuan, JiLin : 2019.10.11,** many videos recorded.

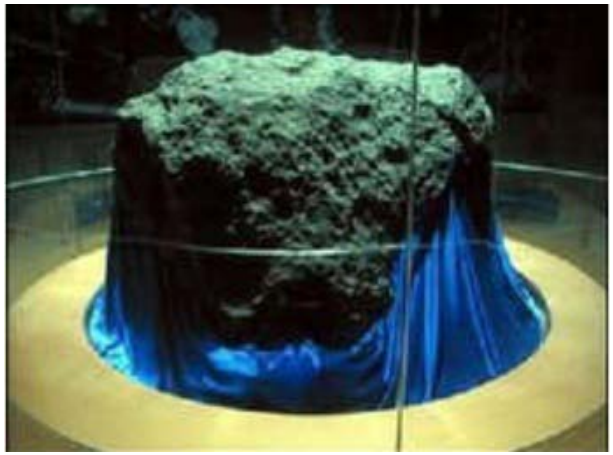

NO.1 meteor in Jilin meteorite event, 1976.3.8

Shangri-La Yunnan, 2017.10.4

1） Earth impact by asteroids

- Velocity : ~20km/s(11.7-73km/s)
- Size : 0.1m-10km

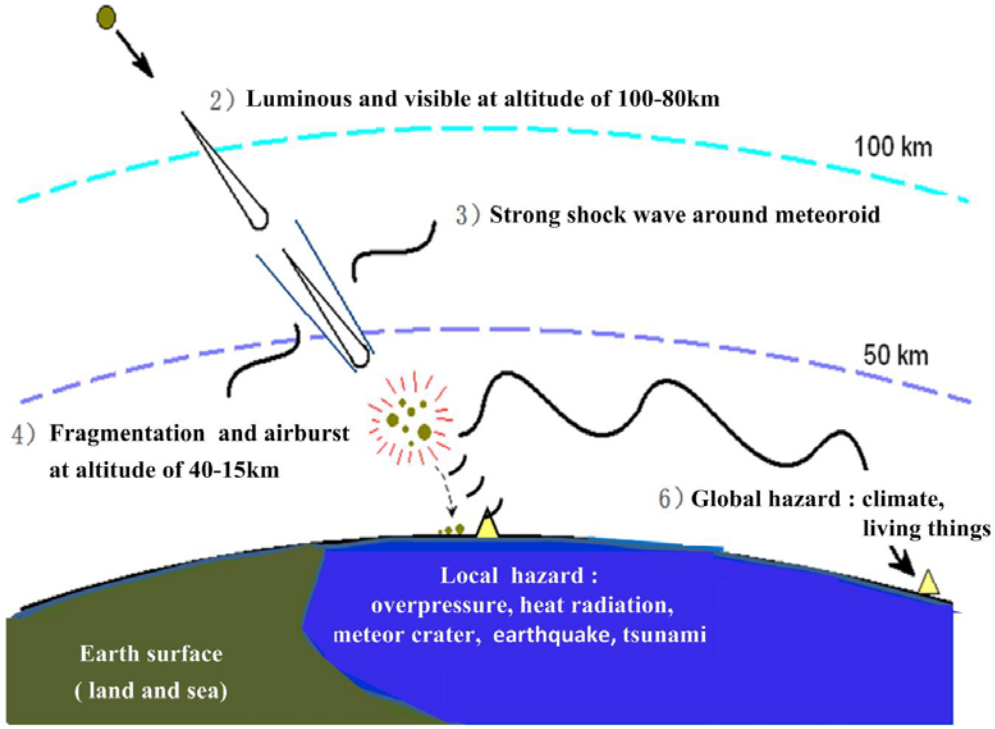

- aerodynamic forces and trajectory during ultra-high velocity entry
- **aerodynamic heating during ultra-high velocity entry**
- ablation and thermal response of asteroid structure
- physical characteristics of asteroid entry process

Earth entry issues in planetary defense

Outline

1、Background

2、Numerical method and physical-chemical model

3、Results and discussion

4、Summary

2. Numerical method and physical-chemical model

- Could the numerical methods and physical-chemical models purposed for reentry vehicles be used in asteroid entry problems?

	Reentry vehicle	Asteroids
Size	<6m	up to several km
Shape	regular , smooth	irregular , unsmooth
Surface Materials	TPS Materials C/H/O/N/Si	Depending on the type（S，M，X） O/S/Si/Fe/Mg/Ca/Na/Al
Interior structure	few defect	cracks, cavities, voids
Entry speed (km/s)	7.5~13	10~70
Peak temperature	≤20000K	~50000K

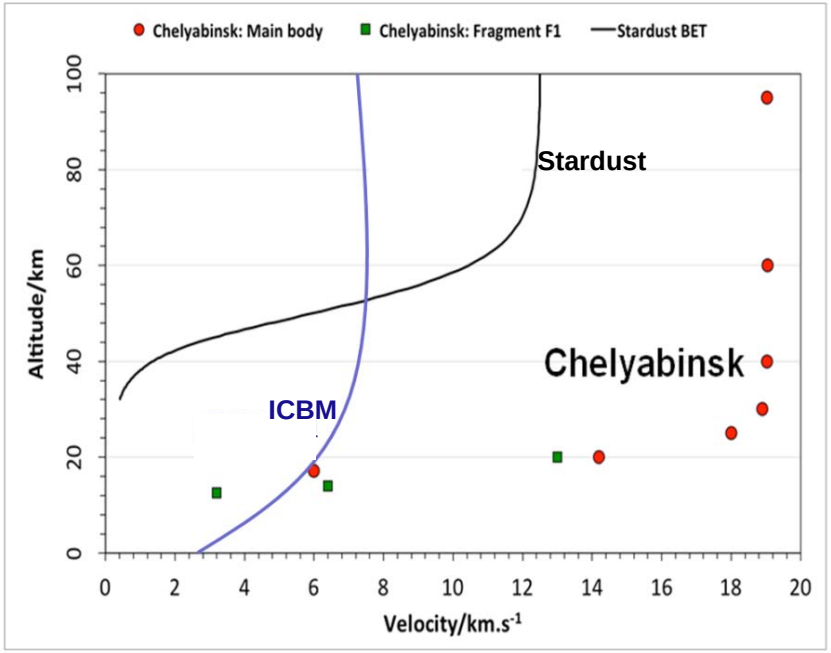

Comparison between the reentry vehicle and asteroid

2. Numerical method and physical-chemical model

- As the primary flow regime of asteroid's entry is continuum-near continuum，the CFD methods might be applicable for asteroid entry calculation；
- However, the physical-chemical models relevant to high temperature gas effects of traditional CFD should be confirmed and improved.

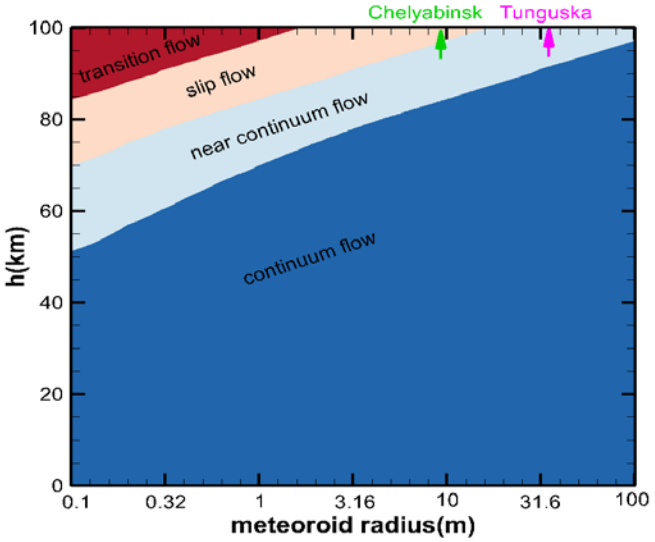

Flow regime of asteroid entry

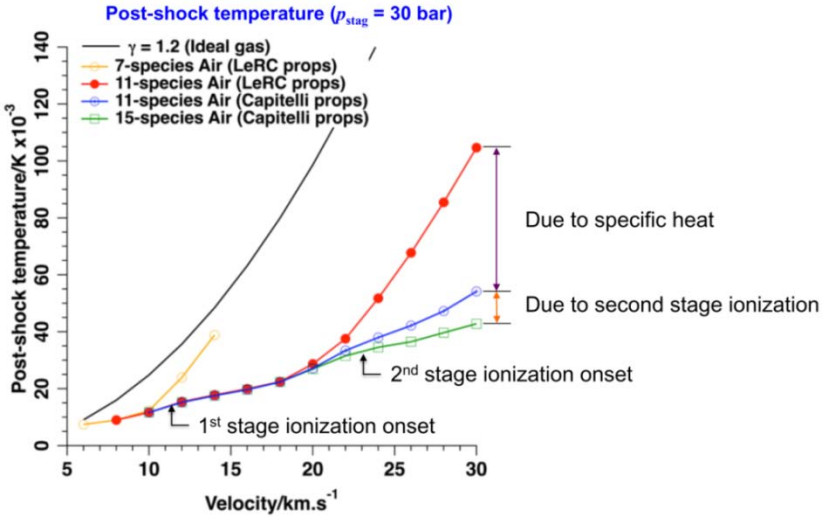

The effect of Air chemical model on post-shock temperature[1]

Ref 1: D.Prabhu.et.al. AIAA SCiTech 2016. Thermophysics Issues Relevant to High-Speed Earth Entry of Large Asteroids

Thermodynamic properties of ultra-high-temperature gas

- Thermodynamics properties of ultra-high-temperature gas are sensitive to the number of electronic states, high-lying level energies and cut-off criteria.
- Thermodynamics properties database valid up to 50,000 K should be constructed for both air species and ablation products.

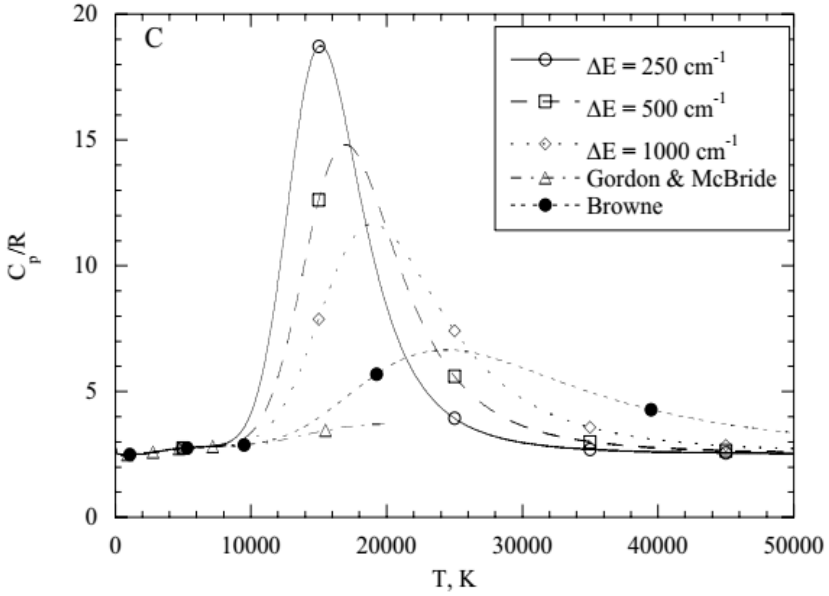

The influence of cut-off criteria on the Cp value of C[2]

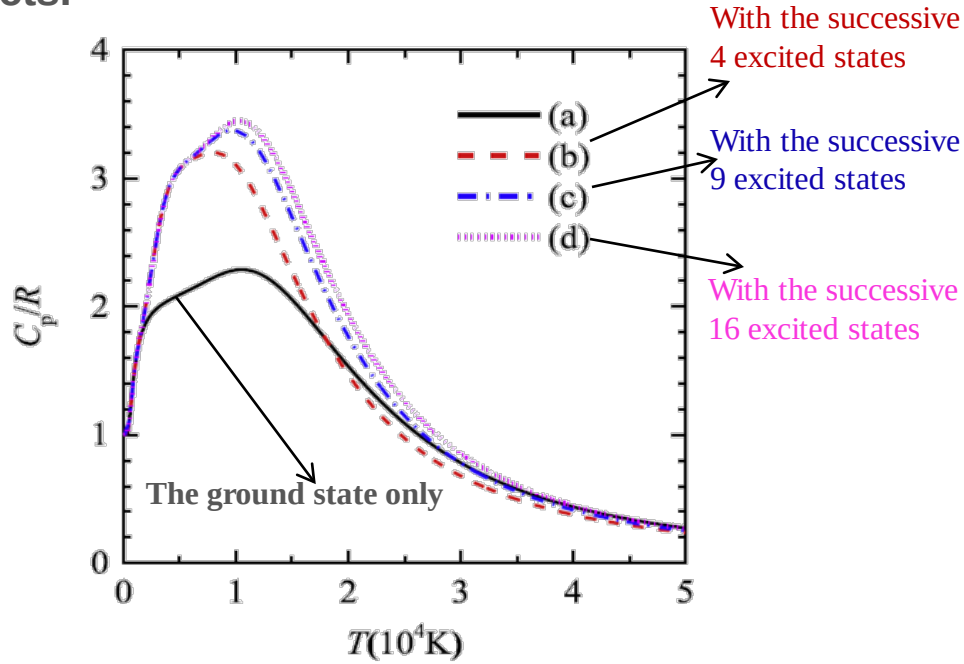

The influence of electronic states on the Cp value of CN[3]

Ref 2: Capitelli.et.al. ESA STR246. Tables of internal partition functions and thermodynamic properties of high-temperature Mars-atmosphere species from 50K to 50000K

Ref 3: Z. Qin .et.al. JQSRT 210 (2018) 1–18 . High-temperature partition functions, specific heats and spectral radiative properties of diatomic molecules with an improved calculation of energy levels

Transport properties of ultra-high-temperature gas

- Based on the Chapman-Enskog method, the collision cross section are needed for transport properties computation.
- high accuracy database of collision cross section up to 50,000 K are needed for both air species and ablation products.

Table 2 Viscosity collision integral $\Omega^{2,2}$ (Å^2) as a function of temperature for neutral–neutral and electron-neutral interactions in air

Interaction	T, K 300	500	600	1000	2000	4000	5000	6000	8000	10,000	15,000	20,000	Acc.,%	Ref.
N_2–N_2	13.72	——	11.80	10.94	9.82	8.70	——	8.08	7.58	7.32	——	——	10	9
N_2–O_2	11.23	——	——	8.36	7.35	6.47	6.21	——	——	5.42	4.94	——	20	5
N_2–NO	13.44	11.87	11.44	10.48	9.32	8.04	7.61	7.27	6.74	6.33	5.62	——	25	24
N_2–N	11.21	——	9.68	8.81	7.76	6.73	——	6.18	5.74	5.36	——	——	10	8
N_2–O	8.99	——	——	6.72	5.91	5.22	5.01	——	——	4.36	3.95	——	20	5
N_2–Ar	11.97	10.50	——	9.28	8.38	7.53	7.25	7.02	6.63	6.32	5.73	——	20	5
O_2–O_2	12.62	11.06	10.65	9.72	8.70	7.70	7.38	7.12	6.73	6.42	5.89	——	20	24
O_2–NO	12.93	11.32	10.90	9.94	8.89	7.80	7.45	7.17	6.73	6.39	5.80	——	25	24
O_2–N	——	8.79	8.47	7.68	6.63	5.67	5.38	5.14	4.78	4.51	4.04	——	25	16
O_2–O	10.13	——	8.61	7.78	6.71	5.67	——	5.13	4.78	4.50	——	——	10	8
O_2–Ar	12.33	10.82	——	9.57	8.54	7.48	7.14	6.87	6.44	6.12	5.54	——	20	5
NO–NO	13.25	11.58	11.15	10.16	9.07	7.91	7.53	7.21	6.73	6.36	5.72	——	20	24
NO–N	——	9.65	9.26	8.29	7.07	5.94	5.60	5.33	4.91	4.60	4.06	——	25	16
NO–O	——	8.79	8.47	7.66	6.64	5.69	5.40	5.17	4.82	4.55	4.08	——	25	16
NO–Ar	13.03	11.33	10.89	9.90	8.85	7.79	7.44	7.15	6.71	6.37	5.77	——	25	24
N–N	9.11	7.94	——	6.72	5.82	4.98	4.70	4.48	4.14	3.88	3.43	3.11	5	15
N–O	9.08	8.15	——	7.09	6.06	5.14	4.88	4.67	4.34	4.07	3.56	3.21	5	15
N–Ar	——	9.31	8.96	8.03	6.84	5.75	5.42	5.17	4.77	4.47	3.95	——	20	16
O–O	9.46	8.22	——	6.76	5.58	4.67	4.41	4.20	3.88	3.64	3.21	2.91	5	15
O–Ar	11.11	10.13	——	8.87	7.69	6.60	6.26	6.00	5.59	5.28	4.74	4.37	20	5
Ar–Ar	12.88	11.12	——	9.66	8.60	7.57	7.23	6.96	6.53	6.20	5.60	5.17	5	24
e–N_2	——	1.46	——	2.07	2.96	3.88	4.09	4.15	4.04	3.85	3.41	3.12	25	28
e–O_2	——	——	——	1.30	1.73	2.10	2.18	2.23	2.29	2.31	2.32	2.31	20	28
e–NO	——	——	——	——	5.64	4.52	4.05	3.73	3.37	3.18	2.92	2.75	35	28
e–N	——	——	——	——	5.68	3.71	3.52	3.42	3.30	3.20	2.95	2.58	35	39, 40
e–O	——	——	——	0.82	1.05	1.34	1.44	1.52	1.65	1.73	1.85	1.90	30	27
e–Ar	——	——	——	0.17	0.30	0.79	1.05	1.31	1.81	2.25	3.07	3.48	15	26

The estimated accuracy of collision cross section data [4]

Ref 4: Wright.et.al. AIAA Journal 43 (2005) 12，2558–2564. Recommended Collision Integrals for Transport Property Computations Part 1:Air Species

Chemical kinetics of ultra-high-temperature gas

- Chemical kinetics models for vehicle entry should not be used directly for asteroid entry.
- New chemical kinetics such as multiple stage ionization、photochemical kinetics and chemical kinetics for asteroid ablation products should be developed.

➢ Chemical kinetics for multiple stage ionization

$$N^+ + e \Leftrightarrow N^{++} + e + e$$

$$O^+ + e \Leftrightarrow O^{++} + e + e$$

➢ Photochemical kinetics

➢ Chemical kinetics for ablation products

[5]

Table 1: Photochemical processes applied in the present study.

#	Process		Spectral Range	Data Source
1	N_2 Photodissociation:	$N_2 + h\nu \leftrightarrow 2N$	9.8 eV $< h\nu$	Stanley and Carlson[30]
2	O_2 Photodissociation:	$O_2 + h\nu \leftrightarrow 2O$	7.1 eV $< h\nu$	Mnatsakanyan[31]
3	N_2 Photoionization:	$N_2 + h\nu \leftrightarrow N_2^+ + e^-$	12.4 eV $< h\nu$	Romanov et al.[32]
4	O_2 Photoionization:	$O_2 + h\nu \leftrightarrow O_2^+ + e^-$	9.7 eV $< h\nu$	Romanov et al.[32]
5	N Photoionization:	$N + h\nu \leftrightarrow N^+ + e^-$	12.4 eV $< h\nu$	TOPbase[33]
6	O Photoionization:	$O + h\nu \leftrightarrow O^+ + e^-$	9.7 eV $< h\nu$	TOPbase[33]

Table 2: Chemical kinetics for meteor ablation products.

i	Reaction	$A_{f,i}$	$n_{f,i}$	$D_{f,i}$	Ref.
1	$Si + e^- \leftrightarrow Si^+ + e^- + e^-$	2.5e+34	-3.82	9.46e+4	Based on N rate[17]
2	$Fe + e^- \leftrightarrow Fe^+ + e^- + e^-$	2.5e+34	-3.82	9.17e+4	Based on N rate[17]
3	$Mg + e^- \leftrightarrow Mg^+ + e^- + e^-$	2.5e+34	-3.82	8.87e+4	Based on N rate[17]
4	$Si + NO \leftrightarrow SiO + N$	3.2e+13	0.0	1775.0	Mick et al.[38]
5	$Si + O_2 \leftrightarrow SiO + O$	2.1e+15	-0.53	16.83	Le Picard et al.[39]
6	$SiO + M \leftrightarrow Si + O + M$	4.0e+14	0.0	9.56e+4	Estimate
7	$SiO_2 + M \leftrightarrow SiO + O + M$	4.0e+14	0.0	9.56e+4	Estimate
8	$Fe + O_2 \leftrightarrow FeO + O$	1.3e+14	0.0	1.02e+4	Akhmadov et al.[40]
9	$Mg + O_2 \leftrightarrow MgO + O$	5.1e+10	0.0	0.0	Hodgson and Mackie[41]
10	$SO + O \leftrightarrow S + O_2$	2.4e+07	1.51	2.53e+3	Lu et al.[42]
11	$SO_2 + S \leftrightarrow SO + SO$	4.8e+14	0.0	1.08e+4	Murakami[43]
12	$O_2 + SO \leftrightarrow SO_2 + O$	2.3e+12	0.0	3.70e+3	Garland[44]
13	$Al + O_2 \leftrightarrow AlO + O$	2.0e+13	0.0	0.0	Cohen and Westberg[45]
14	$Al + SO_2 \leftrightarrow SO + AlO$	9.6e+13	0.0	2.00e+3	Fontijn and Felder[46]
15	$Al + e\text{-} \leftrightarrow Al^+ + e\text{-} + e\text{-}$	2.5e+19	-0.82	6.94e+4	Based on N rate[17]
16	$NaO + O \leftrightarrow Na + O_2$	2.2e+14	0.0	0.0	Plane and Husain[47]
17	$Na + e\text{-} \leftrightarrow Na^+ + e\text{-} + e\text{-}$	2.5e+19	-0.82	5.96e+4	Based on N rate[17]
18	$Ca + O_2 \leftrightarrow CaO + O$	2.5e+14	0	7.25e+3	Kashireninov et al.[48]
17	$Ca + e\text{-} \leftrightarrow Ca^+ + e\text{-} + e\text{-}$	2.5e+19	-0.82	7.09e+4	Based on N rate[17]

Ref 5: Johnston.et.al. AIAA 2017-4533. Impact of Coupled Radiation and Ablation on the Aerothermodynamics of Meteor Entries

Internal degree relaxation model of ultra-high-temperature gas

- Park's two-temperature model （Ttr-Tve）, Multi-temperature model（Tt-Tr-Tvi-Tel）, State-To-State model.
- model parameter such as vibrational relaxation time need to be validated at ultra-high-temperature.

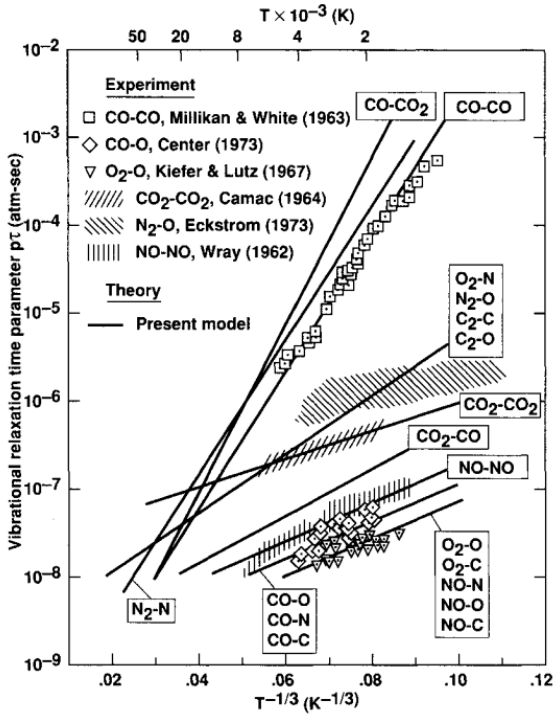

Fig. 2 Comparison between the measured vibrational relaxation times[7,8,51–53] and the present model for carbon-containing species. [6]

Ref 6: Chul, Park.et.al. JTHT 8(1),1994. Review of chemical-kinetic problems of future NASA missions. II - Mars entries.

Radiation model of ultra-high-temperature gas

- Radiation computation: line-by-line method，e.g. NEQAIR.
- Radiation database：TOPbase 、HITEMP. Radiation band of asteroid ablation products should be developed.

Table 3: Summary of molecular band modeling for meteor ablation products[5]

Specie	Transition	Spectral Range (eV)	Data Source
SiO	A-X	4.54-5.79	Franck-Condon factors and energy levels from Geier et al.,[51] and band oscillator strength from Park and Arnold.[52]
SiO	E-X	5.74-7.55	Franck-Condon factors and band oscillator strength taken from Naidu et al.[53] and Drira,[54] and energy levels from Lagerqvist.[55]
FeO	Orange	1.68-2.38	Oscillator strengths and energy levels taken from Michels.[56]
MgO	B-A	1.72-2.45	Oscillator strengths and energy levels taken from Daily[57] and Bell et al.[58]
MgO	D-A	1.72-2.45	Oscillator strengths and energy levels taken from Naulin et al.[59] and Bell et al.[58]
MgO	B-X	2.38-2.69	Oscillator strengths and energy levels taken from Daily[57] and Bell et al.[58]
CaO	A-X	1.1-2.0	Oscillator strengths and energy levels taken from Doherty[60] and Liszt.[61]
CaO	B-X	2.6-3.7	Oscillator strengths and energy levels taken from Pasternack[62] and Liszt.[61]
CaO	Orange	1.7-2.2	Oscillator strengths and energy levels taken from Pasternack[62] and Liszt.[61]
CaO	Green	1.7-2.2	Oscillator strengths and energy levels taken from Pasternack,[62] Liszt,[61] and Baldwin.[63]
SO	A-X	3.8-5.0	Franck-Condon factors and band oscillator strength taken from Borin[64] and energy levels from Rosen.[65]
AlO	B-X	2.2-3.0	Oscillator strengths and energy levels taken from Borovicka.[66]

Ref 5: Johnston.et.al. AIAA 2017-4533. Impact of Coupled Radiation and Ablation on the Aerothermodynamics of Meteor Entries

AHENS

- The CFD code AHENS , developed at our institute for aerothermal environment simulation, solves the NS equations on structured grids.

Numerical Method

- The finite-volume method is used to discretize the governing equations.
- Hybrid Steger-Warming and Godunov flux scheme with second-order spatial accuracy.
- LU-SGS implicit algorithm for time step iteration.
- MPI based parallelism.

High-temperature Gas Model

- 1T / 2T /3T Multi-species gas mixture model.
- Finite-rate chemistry model.
- Polynomial fitting method for thermodynamic properties.
- Gupta's model with collision cross section data for transport coefficients.
- Modified Fick's model for mass diffusion.

$$J_{s\neq e} = -\rho D_s \nabla Y_s - Y_s \sum_{r\neq e} -\rho D_r \nabla Y_r \qquad J_e = -\frac{1}{q_e} \sum_{s\neq e} q_s J_s$$

It ensures that the sum of mass fluxes is zero.

Boundary condition

- Freestream inflow, extrapolation outflow, symmetry.
- RCS jet boundary condition, stagnation boundary condition.
- Unslip or slip boundary condition.
- Isothermal wall or radiative equilibrium wall condition.
- Quasi steady ablation with finite-rate surface chemistry .
- Catalytic wall conditon: non-catalytic , super-catalytic, specified catalytic coefficients.

Radiation model

- Non-Boltzmann models for diatomic molecules and atomic species electronic state populations
- Line information and cross-sections following the work of Johnston.[7]

Molec.	Transition	Name	Spectral Range (eV)
N_2	$B^3\Pi_g - A^3\Sigma_u^+$	1^+ (1^{st}-positive)	0.2 - 2.5
N_2	$C^3\Pi_u - B^3\Pi_g$	2^+ (2^{nd}-positive)	2.7 - 4.7
N_2	$c_4{}'^1\Sigma_u^+ - X^1\Sigma_g^+$	Carroll-Yoshino	11.5 - 14.0
N_2	$c_3{}'^1\Pi_u - X^1\Sigma_g^+$	Worley-Jenkins	11.5 - 14.0
N_2	$b^1\Pi_u - X^1\Sigma_g^+$	Birge-Hopfield I	7.0 - 13.1
N_2	$b'^1\Sigma_u^+ - X^1\Sigma_g^+$	Birge-Hopfield II	7.6 - 14.0
N_2	$o_3{}^1\Pi_u - X^1\Sigma_g^+$	Worley	10.4 - 14.0
N_2^+	$B^2\Sigma_u^+ - X^2\Sigma_g^+$	1^- (1^{st}-negative)	1.2 - 4.6
NO	$B^2\Pi_r - X^2\Pi_r$	β (beta)	2.1 - 6.9
NO	$A^2\Sigma^+ - X^2\Pi_r$	γ (gamma)	3.2 - 7.5
NO	$C^2\Pi_r - X^2\Pi_r$	δ (delta)	3.7 - 7.6
NO	$D^2\Sigma^+ - X^2\Pi_r$	ε (epsilon)	3.4 - 8.0
NO	$B'^2\Delta - X^2\Pi_r$	β' (beta-prime)	3.9 - 8.4
NO	$E^2\Sigma^+ - X^2\Pi_r$	γ' (gamma-prime)	4.6 - 8.9
O_2	$B^3\Sigma_u^- - X^3\Sigma_g^-$	Schumann-Runge	2.6 - 7.0

molecular band systems

Ref 7: Johnston. Nonequilibrium shock-layer radiative heating for Earth and Titan entry[D].PhD Thesis.

Radiation Transfer

- **Radiative Transfer Equation：**

$$\frac{dI_\nu(s,\Omega)}{ds} = j_\nu(s) - \kappa_\nu'(s) I_\nu(s,\Omega)$$

- **Tangent Slab approximation:**

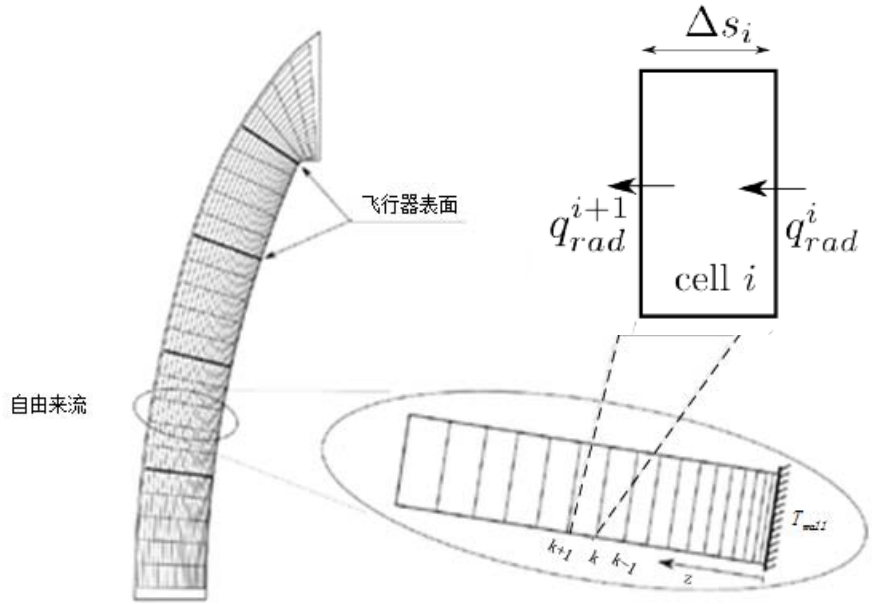

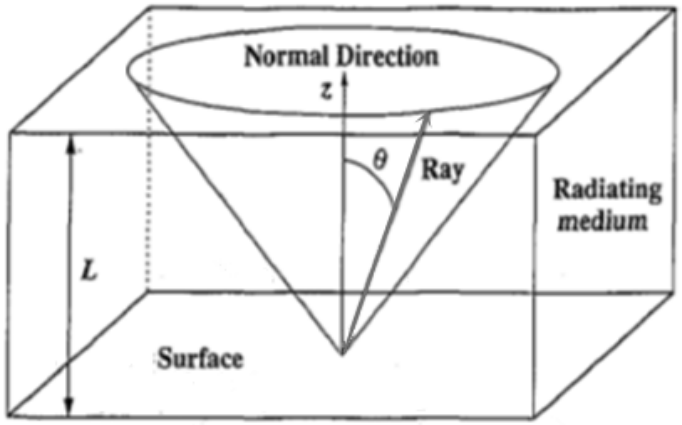

$$-(\nabla \cdot \vec{q}_{\text{rad}})_i = -\left(\frac{\partial q_{\text{rad}}}{\partial s}\right)_i \approx \frac{-\left(q_{\text{rad}}^{(i+1)} - q_{\text{rad}}^{(i)}\right)}{\Delta s_i}$$

Loosely coupled approach

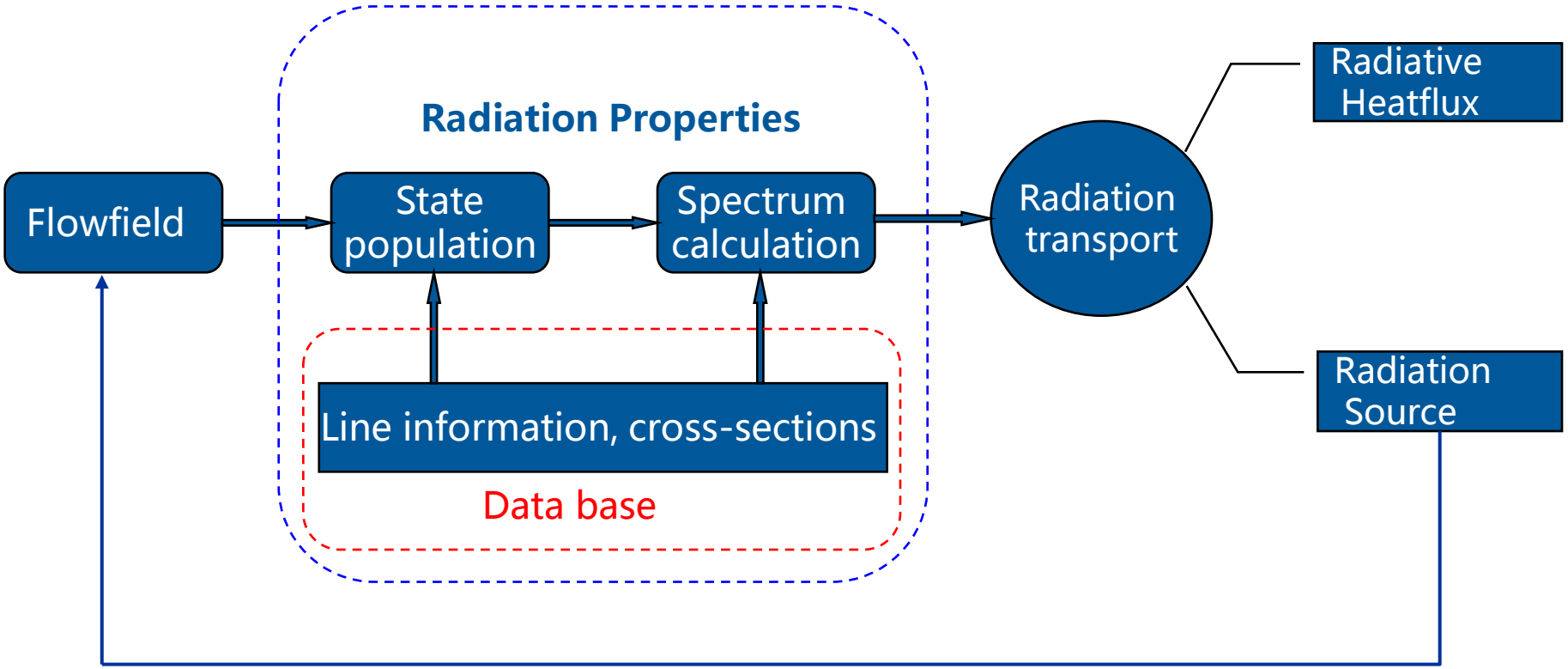

Coupled simulation of flow and radiation

Outline

1、Background

2、Numerical method and physical-chemical model

3、Results and discussion

4、Summary

Stardust vehicle reentry

- The radiation-flow coupling effect is relatively small to the flowfield of the reentry vehicle.

case	H(km)	Voo(m/s)	AoA(°)	Wall conditon
1	59.77	11136.7	0	super-catalytic

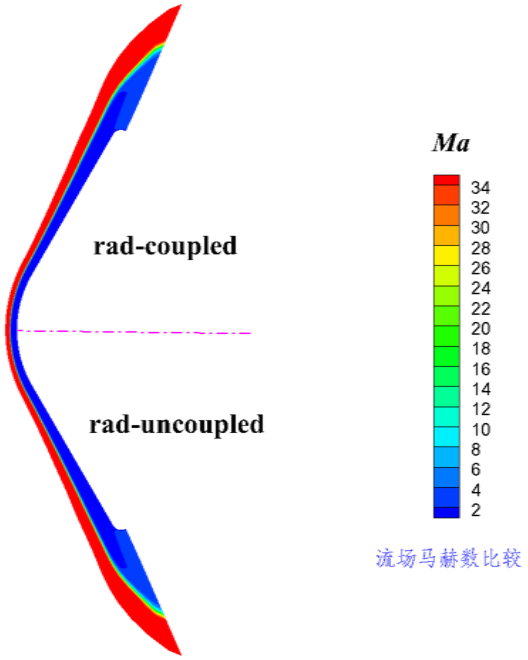

流场马赫数比较

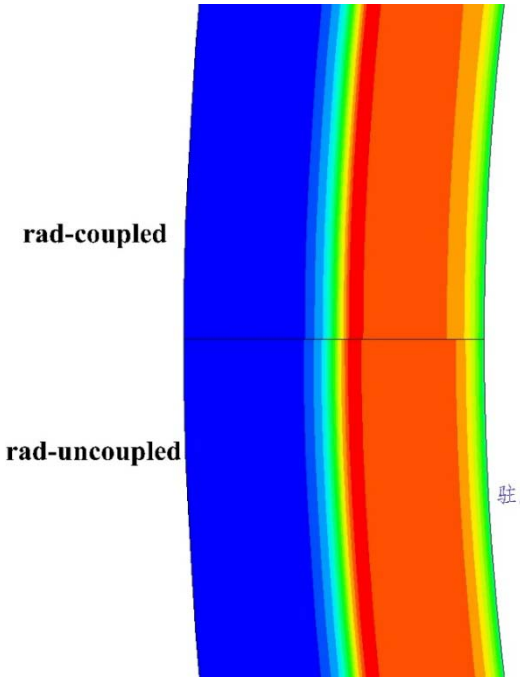

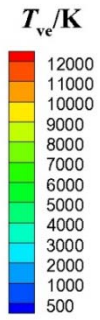

驻点附近振动-电子温度比较

Comparison of the predicted flow properties

Stardust Capsule reentry

- The convective is the dominated mechanism of aerodynamic heating for reentry vehicles, un-coupled radiation simulation can be adopted.

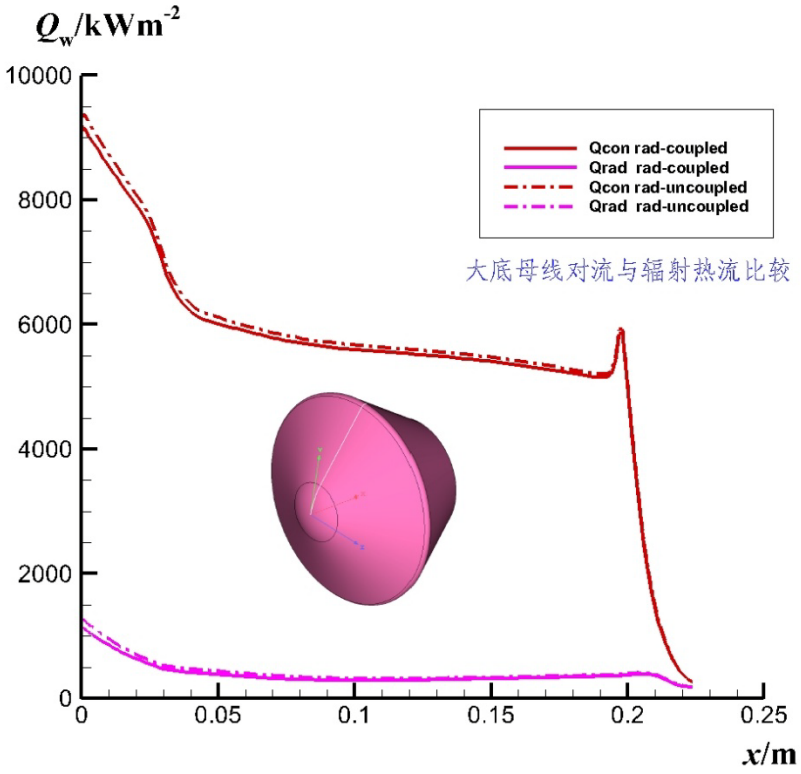

Comparison of the predicted heat flux

Asteroid entry

- Coupled and uncoupled radiation simulations are carried out for typical asteroid entry condition to investigate the influence mechanism radiation-flow coupling on aerodynamic heating.

- A 13 species (N2,O2,N,O,NO,NO+,N2+,N+,N++,O2+,O+,O++,e-) ionized air model is incorporated. [8]

case	H(km)	Voo(km/s)	Wall conditon	D(m)
1	50	15、20	super-catalytic	20
2	50	15、20	super-catalytic	50
3	50	15、20	super-catalytic	100
4	50	15、20	super-catalytic	140

Ref 8: Johnston.et.al. Aerothermodynamic Characteristics of 16-22 km/s Earth Entry[R]. AIAA 2015-3110, 2015.

Asteroid entry

- Radiation-flow coupling effect plays a significant role in flow structure of asteroid entry.
- Compared with uncoupled case, the temperature and thickness of shock layer are much smaller.

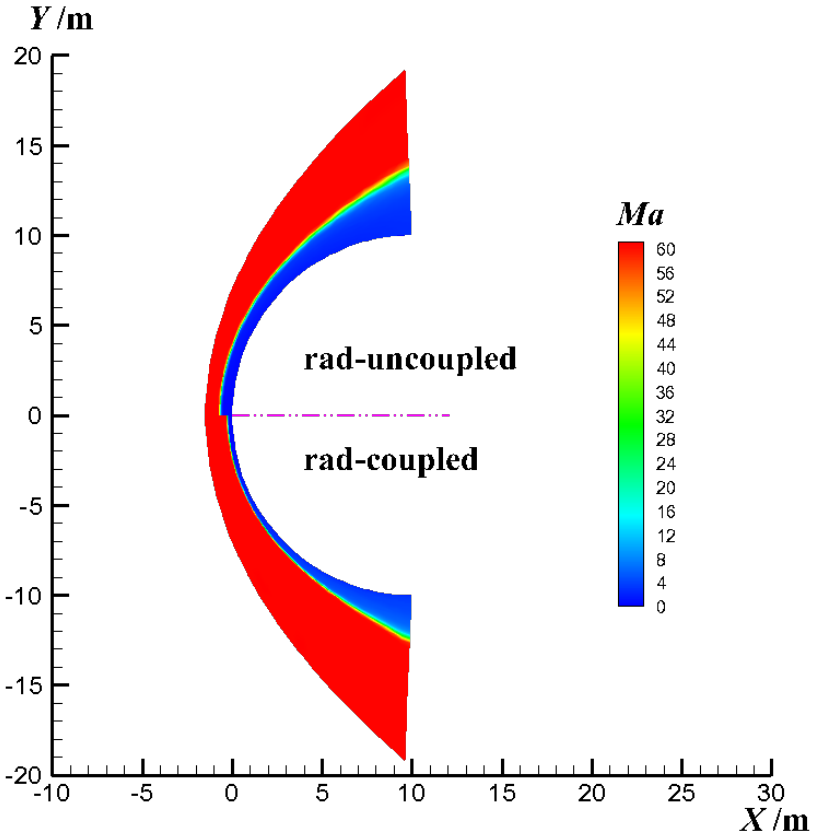

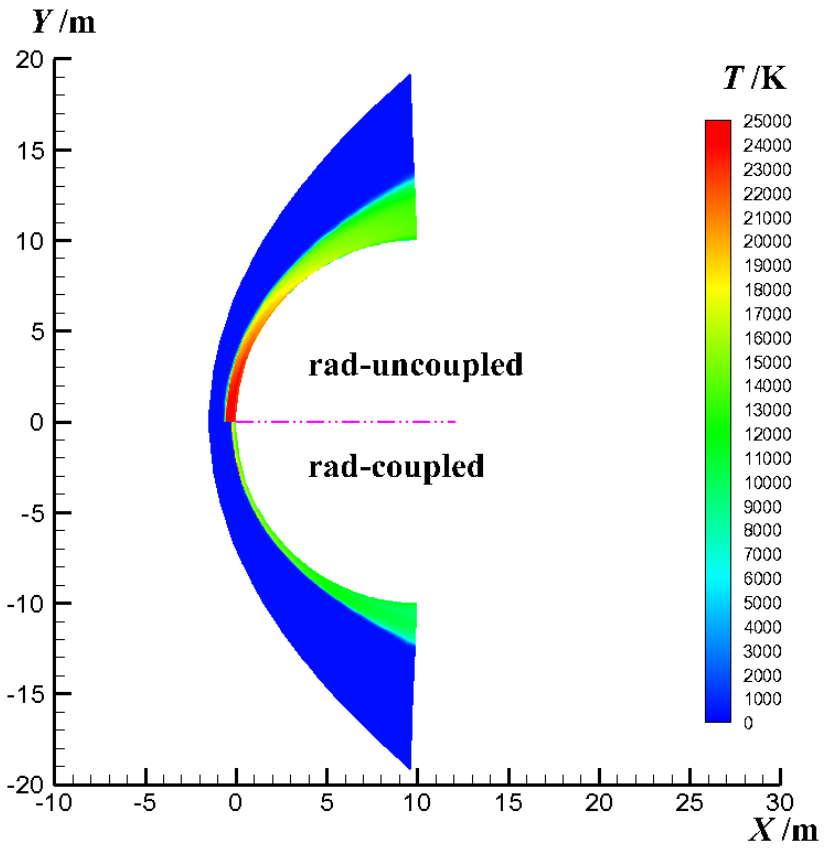

D=20m,V=20km/s

Asteroid entry

- With the increase of entry velocity, the coupling effects on flowfield is enhanced, and the variations of shock standoff distance and peak temperature are enlarged.

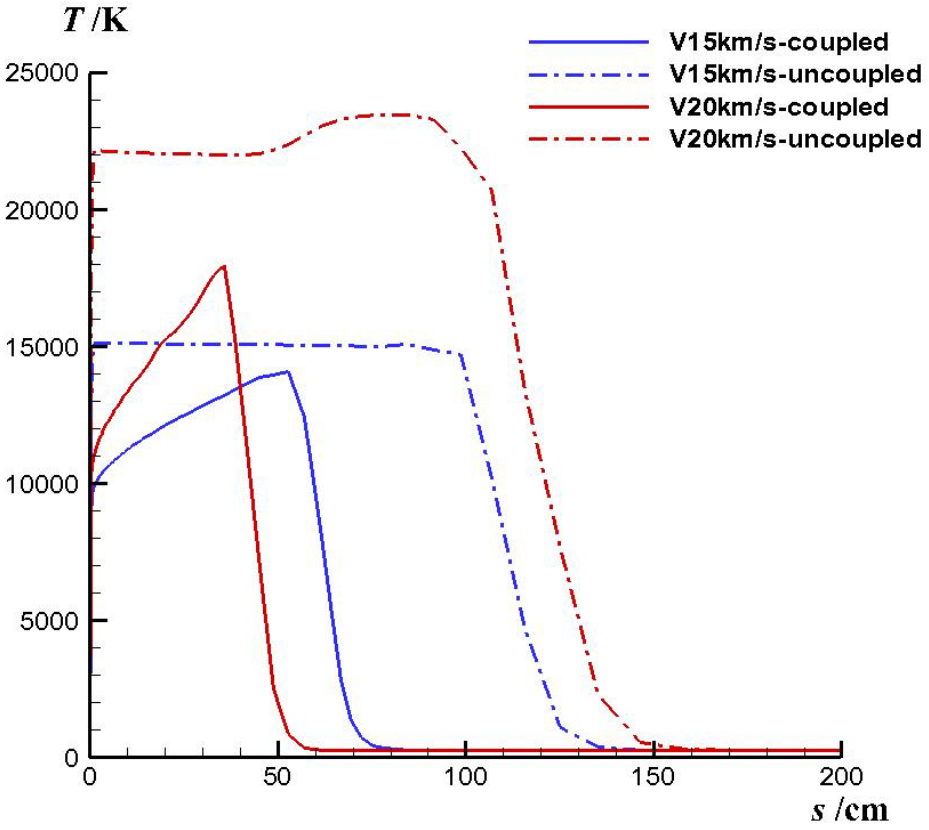

Flow temperature along stagnation line(D=50m)

Asteroid entry

- The radiative cooling and thin shock layer are the physical mechanism that radiation-flow coupling will ease aero-heating.

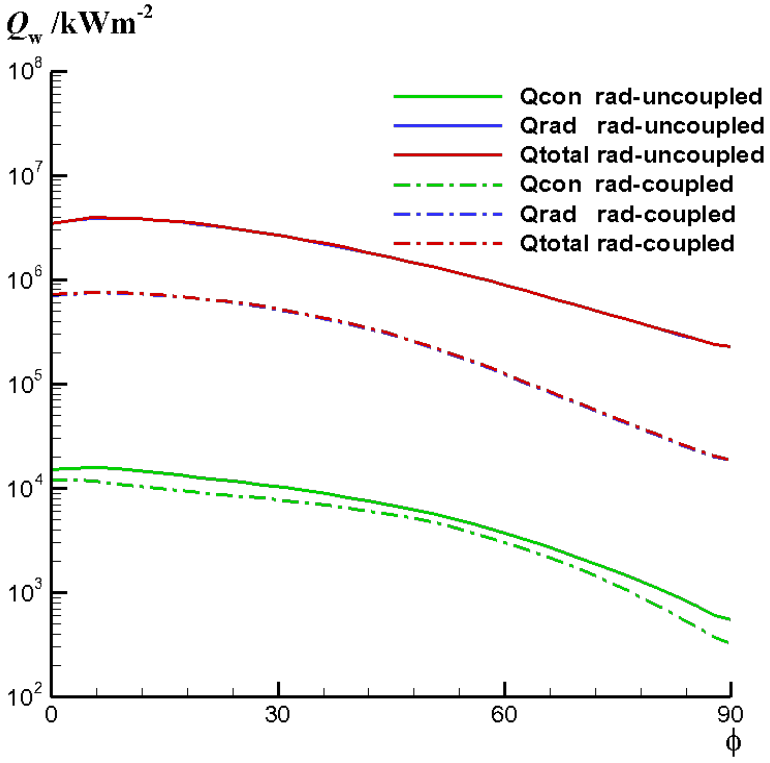

D=20m,V=20km/s

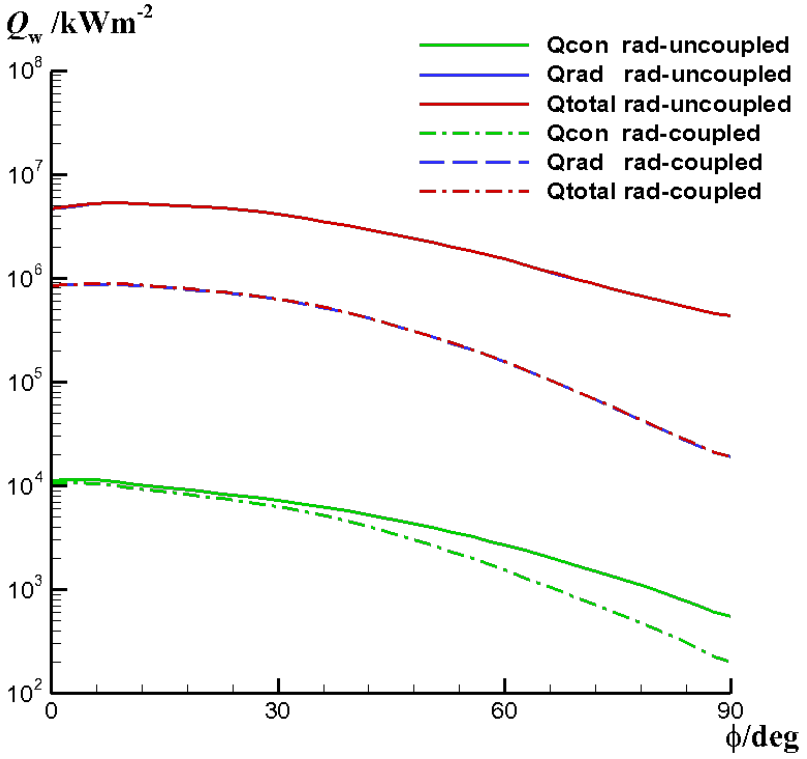

D50m,V=20km/s

Heatflux along surface

Asteroid entry

- There are obvious differences of heating character between asteroid entry and hypersonic vehicle reentry:
- The radiative heating is dominant for asteroid entry and the convective heating is negligible.
- Total heat flux at stagnation point increases with diameter.

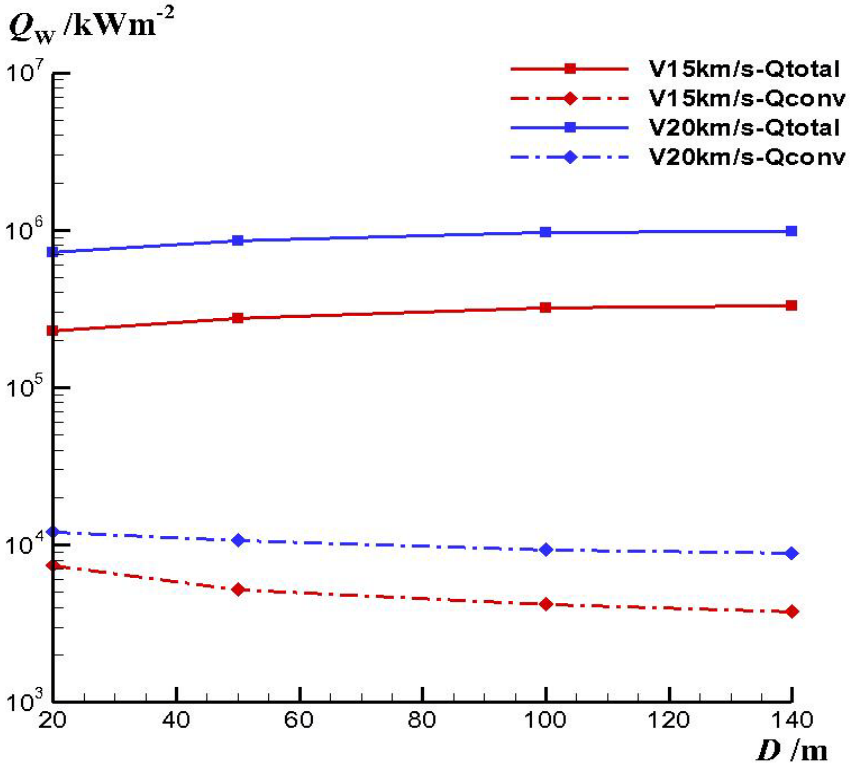

Stagnation point Heatflux

Outline

1、Background

2、Numerical method and physical-chemical model

3、Results and discussion

4、Summary

(1) Hypervelocity aerothermodynamics plays an important role in the analysis of asteroid impacting the Earth.

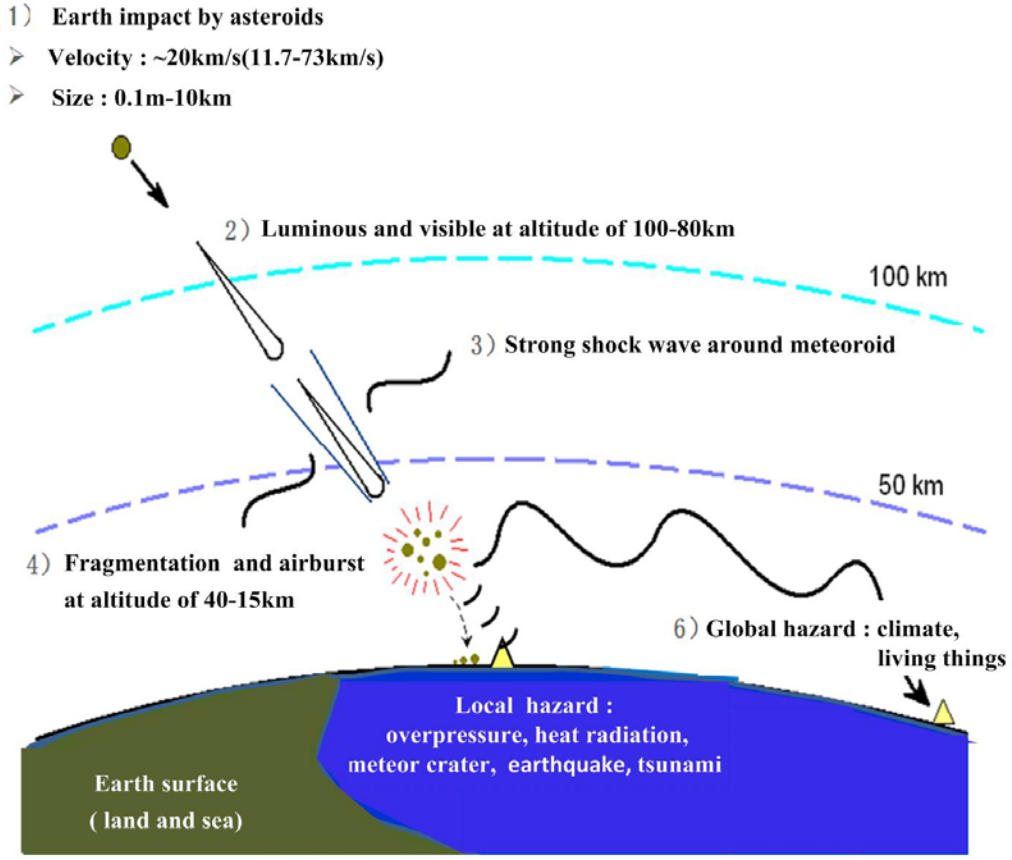

- aerodynamic forces and trajectory during ultra-high velocity entry
- aerodynamic heating during ultra-high velocity entry
- ablation and thermal response of asteroid structure
- physical characteristics of asteroid entry process

4. Summary

(2) In order to investigate the aerothermodynamic problems in asteroid entry to Earth, the high temperature gas models, such as thermo-chemical models and radiation data, need to be extend to greater than 20000K.

(3) Since there are strong coupling effects among flow-field, radiation and ablation in Earth entry problem of asteroid, both the coupling mechanism and numerical methods are needed to be further explored.

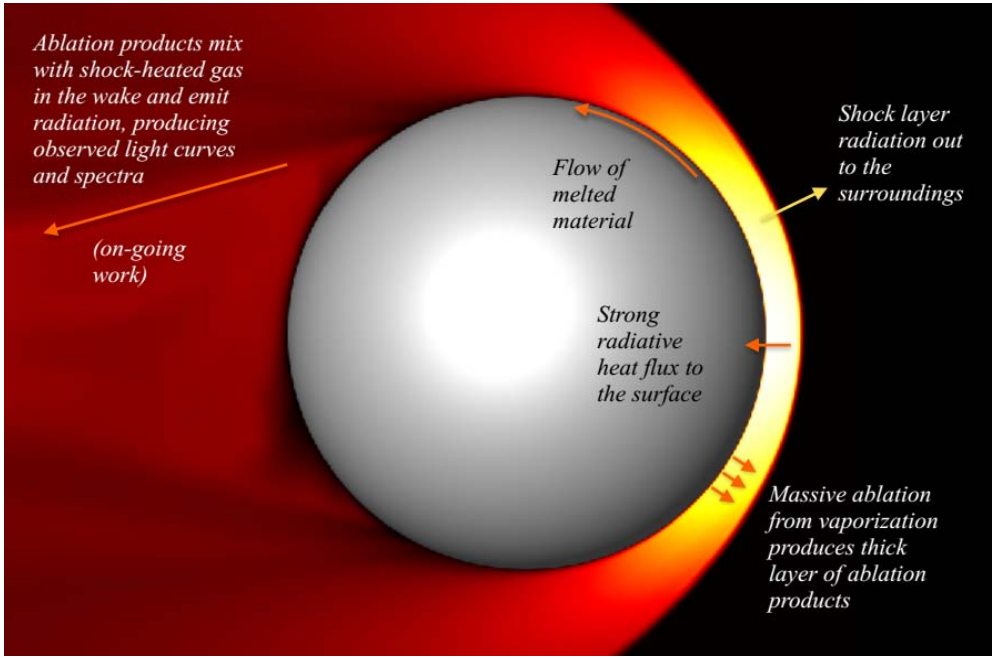

The coupling between asteroid entry flow, radiation and ablation [7]

Ref 9: Eric Stern.et.al. Entry Modeling for Asteroid Threat Assessment

Thanks for your attention

Hypervelocity Aerodynamics Institute of China Aerodynamics Research and Development Center